Journal of Applied Physics

RESEARCH ARTICLE | APRIL 16 2025

Magnonic analog of a metal-to-insulator transition in a multiferroic heterostructure

P. Micaletti ; A. Roxburgh ; E. Iacocca ; M. Marzolla ; F. Montoncello

J. Appl. Phys. 137, 153906 (2025)
https://doi.org/10.1063/5.0250690
CHORUS

Journal of Applied Physics ARTICLE pubs.aip.org/aip/jap

Magnonic analog of a metal-to-insulator transition in a multiferroic heterostructure

Cite as: J. Appl. Phys. **137**, 153906 (2025); doi: 10.1063/5.0250690
Submitted: 26 November 2024 · Accepted: 31 March 2025 ·
Published Online: 16 April 2025

P. Micaletti,[1] A. Roxburgh,[2] E. Iacocca,[2] M. Marzolla,[3] and F. Montoncello[1,a)]

AFFILIATIONS

[1]Dipartimento di Fisica e Scienze della Terra, Università di Ferrara, Ferrara, Italy
[2]Department of Physics and Energy Science, University of Colorado at Colorado Springs, Colorado Springs, Colorado 80918, USA
[3]Dipartimento di Informatica–Scienza e Ingegneria, Università di Bologna, Bologna, Italy

[a)]**Author to whom correspondence should be addressed:** montoncello@fe.infn.it

ABSTRACT

We show how, by changing the polarization value of ferroelectric domains, it is possible to tune the magnon conductivity in the ferromagnetic film layer of a multiferroic magnonic system. In particular, we suggest how to switch from a metal behavior (zero frequency gap and linear frequency-wavevector dispersion) to an insulator behavior (around 1 GHz frequency gap and parabolic dispersion). The ferroelectric film is prepared with a sequence of ferroelectric domains with a periodic variation of their polarization direction. Through inverse magnetostriction, they induce in the ferromagnetic layer a periodic magnetic anisotropy and a consequent sinusoidal magnetization. The amplitude of the sinusoidal magnetization can be varied by varying the induced magnetic anisotropy. This allows for a fine and reversible control over the curvature of the dispersion relations at the Brillouin zone boundary, as well as the width of the frequency gap. We suggest the extension of Dirac's magnon picture to our system, finding interesting implications in terms of magnon mobility. This work expands the possible implementations of the voltage-controlled-bandgap meta-materials, marks the conditions for the occurrence of a magnonic metal behavior in a ferromagnetic film, and outlines how a same unpatterned film can be reversibly turned from a magnonic metal to a magnonic insulator.

I. INTRODUCTION

The voltage/electric field control of ferromagnetic (FM) systems is considered central for future low-dissipation, miniaturized devices.[1–3] The coupling of a ferromagnetic film to a ferroelectric substrate with regular ferroelastic stripe domains is a well known technique to control ferromagnetic properties by voltage or electric fields.[4–7] The combination of strain transfer and inverse magnetostriction in this bilayer system causes the imprinting of magnetic stripe domains in the ferromagnetic layer, and the coupling is proportional to the domain polarization, which can be controlled by an external electric field.[8–11] In general, the manipulation of magnons at the nanoscale through the vertical coupling in multilayers is considered one of the most promising and current research topics, falling into the field of 3D magnonics.[12–15]

Another research effort explores the occurrence of a magnonic frequency gap in magnetic meta-materials as it is fundamental to many applications like filters or mirrors.[16–19] A magnonic bandgap prevents magnon propagation along some direction for some frequencies, acting as a filter. If the gap is independent of the direction, we have a full bandgap and an omnidirectional filter. In a compound system, magnons coming along a waveguide can be perfectly reflected at the interface with a material with a frequency bandgap.[20–22] In analogy with electrons in solids, a magnonic meta-material can be seen as a conductor or insulator for magnon propagation depending on the occurrence of a magnonic gap along the magnon propagation direction. However, in principle, even a uniformly magnetized film is a conductor for magnon propagation, only it has no periodicity and no band structure. Hence, to mark the difference, a magnonic conductor, which is also an artificial crystal (i.e., with a periodic modulation of any of its geometric or magnetic properties), can be referred to as *magnonic metal*, similarly to an electric conductor when consisting of atoms arranged in a crystal structure.

In a ferroelectric/ferromagnetic (FE/FM) bilayer system, the vertical coupling between the layers is the inverse magnetostriction interaction, the intensity of which can be tuned by varying the FE domain polarization through an electric field.[23–25]

In this work, we simulate the inverse magnetostriction by introducing a periodically modulated uniaxial anisotropy K_u in a FM film. The periodicity is attained by a suitable orientation of the ferroelectric domain polarization, and the magnetic anisotropy in the ferromagnetic layer follows suit. We found that as far as the anisotropy coefficient K_u is not too large, specifically below $10^5\,\mathrm{J/m^3}$, after relaxation the magnetization in the FM layer is in a continuous sinusoidal distribution [Fig. 1(a)], with a spatial amplitude Y_0, which depends on the intensity of K_u. Y_0 is related to the magnetization components at the origin [Fig. 1(b)] by the following relation:

$$Y_0 = \frac{m_y^0}{m_x^0}\frac{a}{2\pi}. \tag{1}$$

For instance, at a relative magnetization amplitude $m_y^0/m_x^0 = 1.0$, and for a lattice constant a=256 nm, the spatial undulation amplitude would be 40.8 nm. This information might be useful either when designing the structure or characterizing it by magnetic-force-microscopy/space-resolved magnetic-optic-Kerr-effect. As our ultimate purpose, we aim to present the magnetization undulation as an effective method to create an artificial magnonic crystal, which can be reversibly turned from metal to insulator and vice versa by playing with just a single control parameter. Our technique is based on considering a multiferroic bilayer, with the FE layer prepared in a periodic alternation of the domain polarization. By inverse magnetostriction, the vertical coupling determines a sinusoidal magnetization distribution in the FM layer, producing an interesting magnon dynamics. The undulation amplitude Y_0 can be tuned by varying the anisotropy coefficient K_u, which, in turn, is controlled through an electric field acting on the FE domain polarization and in principle playing as the ultimate control parameter. Hence, we will demonstrate that, in contrast to artificial-spin-ice/straight film hybrids, where only weakly dispersive curves and hardly tunable gaps were found,[14,26,27] this simple strategy provides significant and easily tunable dispersion curve slopes and frequency gaps.

Furthermore, we prove a very challenging effect, namely, the possibility to switch to zero the frequency gap preserving the system periodicity, and at the same time change the dispersion curve at the Brillouin zone (BZ) boundary from parabolic to linear (and vice versa). Note that, in these systems with sinusoidal magnetization, we find that the vanishing of the gap is inevitably concurrent with the linearity of the dispersion curves at zone boundary, which form a distinctive "X" shape, as it happens in graphene at K-point. Since zero gap and linear dispersion curve are traditionally associated to *free propagation* such as electrons in metals, while the presence of a gap and a parabolic dispersion to *propagation blockage* such as electrons in insulators, we might address this as a reversible magnonic *metal-to-insulator transition*.

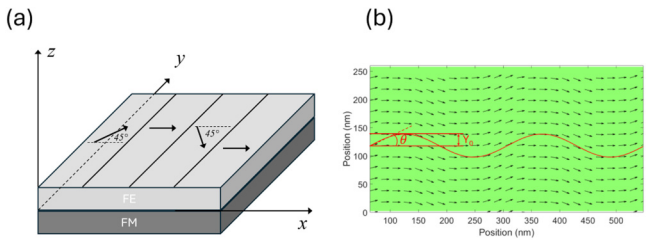

FIG. 1. (a) Scheme of the ferroelectric/ferromagnetic (FE/FM) bilayer, limited to the primitive unit cell, with the indication of the direction of the FE domain polarization. (b) Illustration of the magnetization map (limited to two primitive unit cells) after relaxation, when $K_u = 5 \times 10^4\,\mathrm{J/m^3}$. The sinusoidal distribution has amplitude Y_0, and at the origin, the angle formed by the magnetization vectors is $\theta = \arctan(m_y^0/m_x^0)$, with m_x^0 and m_y^0 magnetization components at the origin.

We will discuss and justify the results of the corresponding simulations within Dirac's magnon approach,[28] which we extend to one-dimensional lattices and continuous medium, finding interesting implications for magnon propagation. Finally, we found that in such a system, the slope of the dispersion curve, i.e., the group velocity v_g, can be tuned through K_u, and, in particular, switched to zero at high K_u values: the same physical system can, hence, be thought of as a versatile device, which can be switched on-demand and in real time (i.e., while magnon is still propagating) from a waveguide (with propagating waves, $v_g \neq 0$) to a dynamic memory (with stationary waves, $v_g = 0$).

This property makes our system in line to the so-called *dynamic* or *reconfigurable* magnonic crystals,[29] where the periodicity of the ferromagnetic medium and its spin waves are controlled (possibly, in real time) by an external parameter (magnetic field,[30–32] current,[33] laser-induced heating,[34] surface-acoustic-wave induced strain,[35,36] etc.). In addition, a further type called *dynamic electromagnonic crystal* was devised in the context of multiferroics, which might recall our work:[5,37–39] here, though, the focus was on the hybridization (coupling) between electromagnetic and spin waves (*electromagnons*) and for this reason even when showing dispersion curves, the focus was mainly on the wavevector range where the coupling occurs ($\sim 10^3$ rad/m[40,41]), and, hence, (depending on the stripe period) around 10^3 times smaller than the range we refer to ($\sim 10^7$ rad/m). Actually, in these papers, the *gap* sometimes refers to the *anticrossing* effect (repulsion) within the coupling region, not only the one due to Bragg's diffraction at zone boundary.[37] These gaps are always very small (~MHz), compared to the ones we found in our simulations (~GHz). To open (and tune) frequency gaps for electromagnons, hence, large stripe periods are used (within $10-800\,\mu$m),[5,38] while we address the nanometric lengthscale ($\ll 1\,\mu$m). Clearly, there are a few similarities with our magnonic framework, but electromagnonic crystals are very different tools with different operating ranges and, hence, with different technological purposes.

In conclusion, under our knowledge, a direct focus on the magnetization undulation and its tunability, the possibility of gradually and reversibly varying the frequency gap from zero to large values (GHz) in a same, unpatterned system, the magnon dispersion curvature (effective mass) were never reported in correlation to each other, particularly in the context of a voltage-control of magnon propagation. For these reasons, we believe that the method of the undulated magnetization offers a solid contribution to the issue of voltage-controlled magnon propagation: our results suggest the use of a magnetization undulation to tune the magnon dispersion curvature and the frequency gap, useful for conceiving versatile spinwave filters and mirrors, waveguides and memories, and

potentially any other innovative magnonic logic devices, enriching the long-established thread of the dynamic magnonic crystals.

II. METHODS AND RESULTS

We perform micromagnetic simulations with the GPU-accelerated micromagnetic simulation program Mumax3.[42] We consider an infinite ferromagnetic film, 5 nm thick, implemented through a square periodic primitive cell with lattice constant $a = 256$ nm and 800 repetitions along the in-plane coordinates (quasi-periodic boundary conditions). The film is discretized with $4 \times 4 \times 5\,\text{nm}^3$ micromagnetic elemental cells. We use permalloy magnetic parameters, namely, saturation magnetization $M_S = 800$ kA/m, exchange stiffness constant $A = 1.0 \times 10^{-11}$ J/m, and gyromagnetic ratio $\gamma = 185$ rad GHz/T. We use a fictitious large damping ($\alpha = 0.9$) to quickly relax to the equilibrium magnetization, while for the excitation process, we use zero damping to allow long lasting precession and, hence, large Fourier coefficients. We divide the primitive cell into four equivalent stripes, where we set a uniaxial magnetic anisotropy with the same magnitude K_u, but different orientation of the easy axis according to the following (periodic) order: 45°, 0°, −45°, 0° [Fig. 1(a)]. In order to obtain frequencies around 10 GHz, we also apply a uniform bias magnetic field $B_0 = 0.1$ T. The film, initially prepared saturated along the x-direction, relaxes to the presence of the bias field and the periodic magnetic anisotropy, and at equilibrium displays a continuous sinusoidal magnetization distribution. This result is found for $K_u \leq 10^5\,\text{J/m}^3$: beyond this value, no regular sine function is found for the magnetization, and instead magnetic domains form inside the primitive cell, with a magnetization almost aligned to the local anisotropy axis, and a sharp discontinuity across each domain. Hence, our investigation is limited to $K_u \leq 5 \times 10^4\,\text{J/m}^3$, which corresponds to an anisotropy field $B_{\text{anis}} \leq 62.5$ mT (in some works, the anisotropy is preferably seen through the associated magnetic field, usually smaller than this value[43,44]).

To compute the dispersion relations, we use a supercell of 200 copies of the primitive cell along the direction of the magnetization undulation (x axis), obtaining a wavevector resolution $\delta k_x \simeq 0.012 \times 10^7$ rad/m. Then, we apply a space–time sinc magnetic field with amplitude 1 mT, cutoff frequency 40 GHz, and wavevector band $k_x = 0.0490$ rad/nm, and save the magnetization map every $\delta t = 25$ ps. Then, we compute the space–time Fourier transform, resulting in the dispersion relation of magnons, with a Nyquist frequency $f_N = 20$ GHz (maximum frequency) and a frequency resolution $\delta f = 0.01$ GHz. On the same magnetization maps, we also compute the time Fourier transform and obtain the space-resolved Fourier coefficients for each frequency and wavevector, i.e., the spin wave (SW) mode profiles. Once chosen a specific frequency, with reference to a point in the dispersion curve map, we plot the real part of the z-component[45] of the dynamic magnetization to visualize the corresponding SW profile.

In fact, SWs in periodic systems are interpreted as Bloch waves, namely, their wavefunction (i.e., the magnetization fluctuation) $\delta\mathbf{m}_\mathbf{k}(\mathbf{r})$ can be expressed as a plane wave times a cell function,[46]

$$\delta\mathbf{m}_\mathbf{k}(\mathbf{r}) = \delta\tilde{\mathbf{m}}_\mathbf{k}(\mathbf{r})\, e^{-i\mathbf{k}\cdot\mathbf{r}}, \tag{2}$$

where $\tilde{\boldsymbol{m}}_\mathbf{k}(\mathbf{r})$ is the SW cell function (which extends over the primitive cell and has the periodicity of the system), $\mathbf{k}$ is the wavevector, and $\mathbf{r}$ is the position across the lattice.

The spin dynamics of a FM film with sinusoidal magnetization is rather simple, as far as the undulation amplitude Y_0 is small, and consists of Bloch waves with a cell function profile having m (or n) nodal lines either perpendicular (backward spin waves, m-BA) or parallel (Damon–Eshbach modes, n-DE) to the undulation direction (x axis).[47–50] Mixed modes, labeled $(m, n) \equiv (m\text{-BA}\times n\text{-DE})$, are also possible. In the reduced scheme of the BZ, the number of nodes (or, equivalently, the mode label) represents the band index for any given wavevector k.[19,46] Since the magnetization flux M oscillates along x axis, we consider only the dispersion along that axis (i.e., backward waves only).

We computed the dispersions at different values of K_u, encompassing four orders of magnitude, from 1×10^1 to $5 \times 10^4\,\text{J/m}^3$. These values are in line with the range reported in the literature about magnetic anisotropy induced by inverse magnetostriction.[9,10,51–54]

In sinusoidally magnetized films, the spin dynamics is invariant with respect to a mirror operation of the magnetization map around the x axis (called σ_h in Ref. 55), i.e., invariant with respect to the inversion of the magnetization component m_y. Hence, even if to plot a sinusoidal distribution of the magnetization we had to consider a *geometric* primitive cell with side $a = 256$ nm, the actual, *physical* primitive cell emerging in the dynamics is only a half of the designed one, namely, $d = 128$ nm. Consequently, the *physical* Brillouin zone boundary occurs at $2 \times \frac{\pi}{a} = 2.45 \times 10^7$ rad/m (twice as big as the geometric one). The output of the simulations confirmed this point (dashed vertical lines in Fig. 2).

In Fig. 2, we show six indicative cases of dispersion curves to illustrate the metal-to-insulator transition and the variation of the gap as K_u is increased.

For any $K_u < 0.04\,\text{kJ/m}^3$ (not shown), the magnetization maintains the uniform saturated state, and the dispersion curve does not show any trace of folding to the reduced Brillouin zone, namely, no periodicity is imprinted on the film nor can its dispersion be distinguished from that of the uniform film ($K_u = 0$). It is a sort of hysteresis under K_u variations: in-plane exchange interaction and the strong out-of-plane dipolar fields are stronger than the anisotropy and continue to keep the film magnetization uniform. This is a remarkable result, since it defines the limit of K_u, below which it is ineffective as a perturbation of the film uniform magnetization: in other words, our simulations suggest that to have evidence for periodicity in the experiments with a real permalloy film (either with metal or insulator behavior), it is necessary to design the ferroelectric overlayer such that it can induce, by vertical coupling, a magnetic anisotropy $K_u \geq 0.04\,\text{kJ/m}^3$. Below that value, the system behaves like an ordinary film without "bands": note that only with "bands" it is possible to increase the magnon frequency by concurrently decreasing the wavevector, which is impossible in the single-valued dispersion curve of a uniform film.

A. Magnon metal

Within the range $0.04 \leq K_u \leq 0.4\,\text{kJ/m}^3$ [Fig. 2(a)], the dispersion curve follows that of the uniformly magnetized film, but now showing the characteristic periodic folding to the reduced Brillouin zone, with no appreciable gap (<0.01 GHz): the dispersion

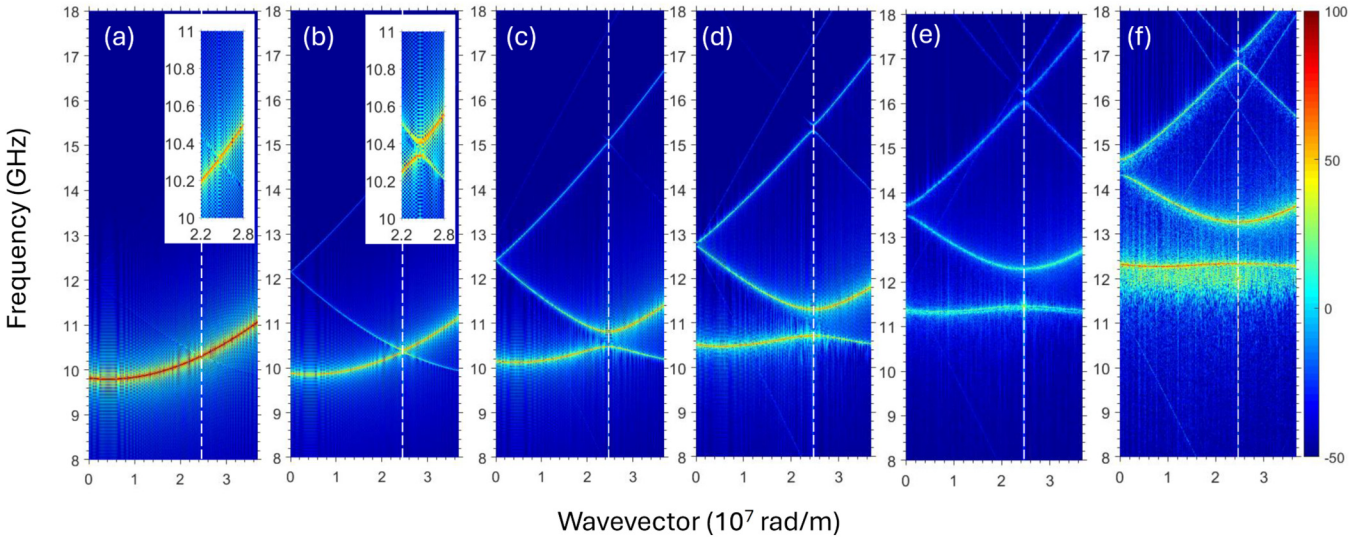

FIG. 2. Dispersion curves along the x axis direction for (a) $K_u = 1.0 \times 10^2$ J/m^3 (metal behavior), (b) $K_u = 1 \times 10^3$ J/m^3 (insulating behavior), (c) $K_u = 5 \times 10^3$ J/m^3, (d) $K_u = 1 \times 10^4$ J/m^3, (e) $K_u = 2 \times 10^4$ J/m^3, and (f) $K_u = 3 \times 10^4$ J/m^3. The insets in panel (a) and (b) magnify, thanks to a different aspect ratio, the region at the Brillouin zone boundary. The blurring in panel (f) is an artifact of the simulation. Note that the results of the simulations, providing the Brillouin zone boundary at $k = 2.45 \times 10^7$ rad/m demonstrate backward that the physical lattice constant is $d = 128$ nm, namely, a half of the geometric one a.

curves cross each other at the Brillouin zone boundary in the distinctive "X" shape, where they show a clear linear behavior. In this condition, magnons can continuously change their frequency (and wavevector) for any arbitrarily small variation of the external driving force operated by the (microwave) antenna: we might address them as "free magnons." This aspect in some way recalls what happens to "free electrons" in metals, where electrons can be put into motion by an arbitrarily small voltage.

Remarkably, variations of K_u in the range at which the system behaves like a magnon metal are not affecting the dispersion curve at all, nor changing it with respect to the uniformly magnetized case (except for the periodic folding). We might draw a first conclusion, that in systems with a sinusoidal magnetization, the group velocity, and the consequent magnon mobility, is robust with respect to K_u variations.

In analogy with metal graphene electrons, it is interesting to translate the reference system origin at the zone boundary point (Dirac's point) where the dispersion curve crosses its reflection to the reduced Brillouin zone, and consider frequency and wavevector within a limited interval across that point. In this context, the usual definition of effective mass[46] is not applicable since the assumption of a parabolic dispersion relation is not appropriate across Dirac's point. In addition, a straight dispersion line would show zero curvature and imply an infinite effective mass, in contrast with the claimed high mobility. In this specific context, being p the magnon momentum and $\hbar$ the reduced Planck's constant, we can write the magnon effective mass as[56]

$$m^* = \frac{p}{v_g} \equiv \frac{\hbar\kappa}{v_g} \equiv \frac{\hbar\kappa}{\frac{\partial\omega}{\partial\kappa}}, \tag{3}$$

where, in fact, $\kappa \equiv k - \frac{\pi}{d}$, so that, with reference to Dirac's point, $\kappa \longrightarrow 0$ implies $m^* \longrightarrow 0$. Equation (3) holds for non-dispersive magnons (i.e., v_g in a linear relationship with k), particularly around the Brillouin zone boundary. A vanishing effective mass implies high mobility (freedom) with respect to the application of an external driving force (which, in the case of magnons, corresponds to variations in frequency and wavevector of the microwave field from the excitation antenna).

In a narrow interval across the BZ boundary, the slope of the two crossing curves is the same, because of the space inversion symmetry of the magnetization undulation along x axis.

Hence, despite having a one-dimensional system, in order to gain information on magnon conductivity, for analogy with electrons in graphene, we might write the dispersion relation (approximately linear in a narrow interval across the BZ boundary) using Dirac's magnon formalism,[28,57,58]

$$\omega_{\pm}(\kappa) = \frac{\epsilon}{\hbar} \pm v_g|\kappa|, \tag{4}$$

where $\omega = 2\pi\nu$ is the magnon pulsation, $\frac{\epsilon}{\hbar} \equiv 2\pi\nu\left(\frac{\pi}{d}\right)$, and the group velocity v_g plays the role of Dirac's velocity. The $\pm$ sign marks the "X" shape of the dispersion. The straight line, passing through frequency $\nu\left(\frac{\pi}{d}\right)$, and locally approximating the dispersion curve at zone boundary, can be more explicitly written as

$$\nu(k) = \frac{d}{\pi}\left[\nu\left(\frac{\pi}{d}\right) - \nu_0\right]k + \nu_0, \tag{5}$$

where d is the physical lattice constant, and, of course, $\nu_0 \equiv \nu(0)$ is not necessarily a real point of the global dispersion curve.

This straight line is at the origin of Eq. (4). In a linear lattice (as the present case), the group velocity is related to the *hopping rate* ν_t by the relation

$$\nu_g = 2\pi\frac{\partial\nu}{\partial k} = 2\pi\frac{d}{\pi}\left[\nu\left(\frac{\pi}{d}\right) - \nu_0\right] = 2\,d\nu_t. \tag{6}$$

Hence, within this picture, the hopping rate is $\nu_t = \nu\left(\frac{\pi}{d}\right) - \nu_0$. Being linked to ν_g, the hopping rate is an indication of the magnon mobility across the lattice, i.e., the rate at which magnons hop from one half of the primitive cell to the next half along x-axis, corresponding either to a translation of $d/2$ or a phase-shift of $\pi/2$. The hopping rate tends to zero when propagation is inhibited (flat dispersions/stationary solutions).

With reference to the zone boundary and Dirac's point, it is possible to consider Dirac's magnons as non-dispersive wave packets. In fact, for $k = \frac{\pi}{d}$, i.e., $\kappa \longrightarrow 0$, if ν_p is the phase velocity (related to the magnon pulsation ω), we have

$$\frac{\partial\nu_p}{\partial\kappa} = \frac{\partial}{\partial\kappa}\frac{\omega(\kappa)}{\kappa} = \frac{1}{\kappa}\frac{\partial\omega(\kappa)}{\partial\kappa} - \frac{\omega(\kappa)}{\kappa^2} = \frac{1}{\kappa}\left(\nu_g - \nu_p\right). \tag{7}$$

In other words, the sinusoidal magnetization makes the film system a Dirac material, where the equivalence $\nu_g = \nu_p$ holds in a wide wavevector interval across the BZ boundary. In this way, the magnon wave packet, once excited, is non-dispersive and can propagate coherently very longer, preserving its momentum (ballistic transport). This property is particularly interesting in the contexts where magnons are used to carry and process information. Since the magnon hopping rate ν_t is associated to the effective information transfer, it might be seen as the gain achieved for any given excitation frequency. The main source for ν_t is the interaction, which, if increased, tends to increase the slope of the dispersion at the Brillouin zone boundary. Since we have a very thin film (5 nm), exchange interaction prevails over the dipolar one, providing BA dispersion curve a positive slope. Actually, exchange tends to stiff the magnetization and oppose spin fluctuations and, hence, to increase the magnon frequency. Furthermore, exchange interaction favors the coherence among the precessing spins over distance and hence the oscillation propagation (in contrast to dipolar interaction, which favors the precession decoherence over distance,[48] and magnetic anisotropy, which tends to reduce ν_g).

In order to give insight about the control over ν_t, using the analytical dispersion relation for dipole-exchange backward spin waves, presented in Ref. 59, we plotted the curves for three systems (Fig. 3) differing in geometrical and magnetic parameters, producing the same frequency (10.32 GHz) at zone boundary but with very different ν_g. The black curve reproduces analytically the exact dispersion curve presented in Fig. 2(a) and found by simulations, only without the folding to the reduced BZ, for simplicity. By linear interpolation, we found a group velocity $\nu_g \simeq 314$ m/s, as well as $\nu_0 = 9.095$ GHz and $\nu\left(\frac{\pi}{d}\right) \equiv \nu(\kappa = 0) = 10.32$ GHz; hence, the hopping rate is in this case $\nu_t = 1.225$ GHz. The red curve is designed to have $\nu_t = \nu\left(\frac{\pi}{d}\right)$ and refers to a 100 nm thick film of a

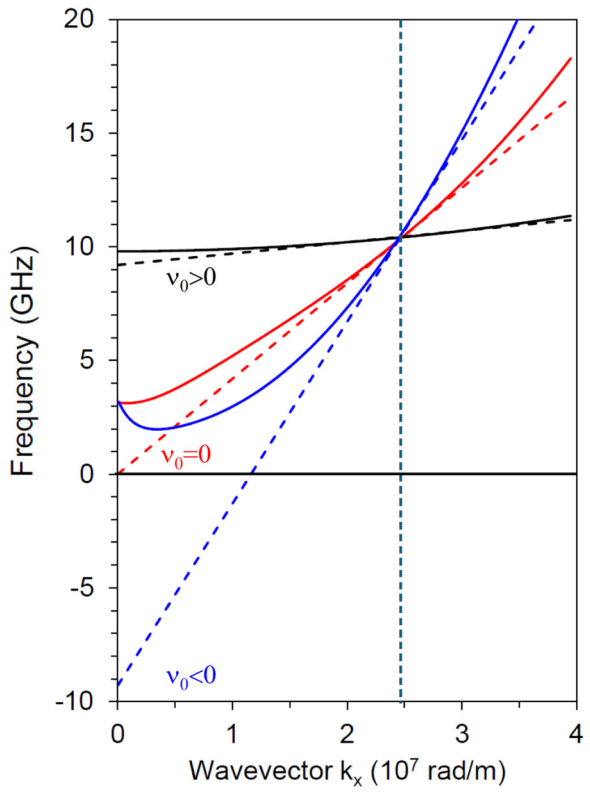

FIG. 3. Dispersion curves $\nu(k)$ for three systems with different geometric and magnetic parameters, with increasing exchange stiffness constant and, hence, hopping rate. The curves are plotted following the analytical backward dispersion relation discussed in Ref. 59, without the periodic folding to the 1st BZ. The dashed straight lines are the tangents to the corresponding dispersion curves at zone boundary (marked by the vertical dashed line): the black one represents a case with $\nu_0 > 0$, and, hence, with low ν_t; the red one has a larger exchange constant and is designed to give $\nu_0 = 0$; the blue one has $\nu_0 < 0$ and, hence, very large exchange constant and ν_t.

fictitious material with $M_s = 900$ kA/m, exchange parameter $A = 14.0 \times 10^{-11}$ J/m and subject to an applied field $B_0 = 10$ mT. Its linear approximation (tangent) at zone boundary is also plotted (dashed red line): $\nu_t \simeq 10.32$ GHz, corresponding to $\nu_g \simeq 2.64$ km/s. The blue curve refers to another fictitious material, designed to have $\nu_t \gg \nu\left(\frac{\pi}{d}\right)$. To compare with the previous curves and keep the same frequency (10.32 GHz) at zone boundary, we used the following parameters: film thickness 1.5 μm, $M_s = 1500$ kA/m, $A = 50 \times 10^{-11}$ J/m, gyromagnetic ratio $\gamma = 150$ rad GHz/T, under a bias field of 10 mT. Its linear approximation (tangent) at zone boundary is shown (dashed blue line): $\nu_t \equiv \nu(\pi/d) - \nu_0 = 19.6$ GHz ($\nu_0 \simeq -9.3$ GHz), corresponding to $\nu_g \simeq 5.02$ km/s.

Dirac's magnon picture, applied to our results, discloses the vast consequences of the approach to a voltage-driven magnon dynamics under a sinusoidal magnetization: to have a *magnonic metal* behavior (i.e., periodicity and bands, with a linear dispersion and no gap at zone boundary), anisotropy is necessary indeed, and

in our case, we found that the anisotropy coefficient must be $K_u \geq 0.04\,\mathrm{kJ/m^3}$. Under these conditions, magnons behave like non-dispersive mass-less wave packets, with a group velocity, and, hence, mobility, which can be designed by an adequate choice of magnetic and geometric parameters (Fig. 3).

The very fact that magnons, in analogy to electrons in solids (and graphene), can be interpreted in wave mechanics in terms of wave packets,[60] stands at the origin of the extension of Dirac's magnon picture to our case, characterized by a linear lattice and a continuous medium. Being wave packets, they possess a phase velocity (associated to the pulsation) and an independent group velocity (associated to the propagation), both determined by the involved interactions. For this reason, we suggest to address a ferromagnetic film, subject to an appropriate periodic anisotropy, as a the magnonic analog of a metal material.

B. Magnon insulator

While we demonstrated that some anisotropy is necessary to have a *magnonic metal* behavior, too much anisotropy turns the material into a magnon insulator. In fact, as $K_u \geq 0.4 \times 10^3\,\mathrm{J/m^3}$ [Figs. 2(b)–2(f)], a frequency gap arises, due to a symmetry breaking in the anisotropy interaction (vertical coupling) experienced by the modes and consequent degeneracy lifting. This also implies that the dispersion curvature increases and becomes parabolic, determining an increase of the magnon effective mass,[46]

$$m^* = \frac{\hbar^2}{\frac{\partial^2 E}{\partial k^2}} \equiv \frac{\hbar}{\frac{\partial^2 \omega}{\partial k^2}}, \tag{8}$$

where this relationship holds for dispersive magnons. In analogy with electrons in solids, in some way, magnons acquire a progressive inertia, which makes them responding less promptly to possible external forces driven by the antenna. In other words, if we need the antenna to excite a specific magnon frequency, a larger m^* implies a larger k, because the dispersion curvature decreases. Likewise, if we need to provide a magnon with a given kinetic energy, a larger m^* would require a larger k as well, since:

$$v_g = \frac{\hbar k}{m^*}. \tag{9}$$

Finally, for any given induced frequency change $\delta\nu$, the wavevector range δk needed in the wave packet increases for increasing m^*.

In a sense, to hop from one half of the unit cell to the other half [in Fig. 4, moving from (a) to (b)], under an external force, magnons are required an extra amount of energy, corresponding to the gap, so that at the BZ boundary a continuous propagation is inhibited and only a stationary wave behavior is possible. This extra energy is increasing with increasing K_u [Figs. 2(c)–2(f)] and is due to the symmetry breaking introduced by the periodic anisotropy: hence, K_u can be used to tune the magnon mobility in real time. For instance, when $K_u = 5 \times 10^3\,\mathrm{J/m^3}$, a simple fit with the corresponding dispersion curve data at the BZ boundary of Fig. 2(c), under a parabolic approximation, gives an effective mass $m^* = 5.59 \times 10^{-27}\,\mathrm{kg}$, i.e. (just to provide a quantitative reference), 6138 times the electron mass. However, if we increase the anisotropy coefficient to $K_u = 2 \times 10^4\,\mathrm{J/m^3}$ [Fig. 2(e)], i.e., 4 times larger, the fit provides $m^* = 11.98 \times 10^{-27}\,\mathrm{kg}$, i.e., slightly more than the double (13153 electron masses). Hence, as the curvature of the upper dispersion curve decreases for increasing K_u (i.e., the parabola becomes wider), the effective mass increases and so does the magnon inertia to speed changes. Note that for $K_u = 5 \times 10^3\,\mathrm{J/m^3}$, the frequency gap is evaluated about 0.380 GHz, while for $K_u = 2 \times 10^4\,\mathrm{J/m^3}$, it is about 0.800 GHz.

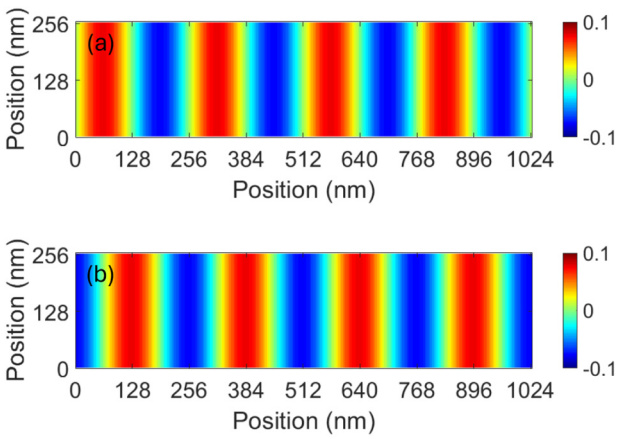

FIG. 4. Mode profiles at the Brillouin zone boundary for the *magnon metal* case $K_u = 1 \times 10^2\,\mathrm{J/m^3}$: (a) F mode (also 0-BA); (b) 1-BA mode. Note that they happen to be indistinguishable provided a translation of $d/2$, and both occur at around 10.3 GHz. In the plot, four geometric BZs are shown ($a = 256$ nm), corresponding to eight physical BZs along x ($d = 128$ nm). The color map indicates the mode amplitude in arbitrary units.

The occurrence of the bandgap is the consequence of the interaction of the spin modes with the periodic anisotropy field (which is the simulation of the inverse magnetoelastic effect in a multiferroic bilayer). The spin modes relevant for the dispersions are, in our case, backward modes of order m (m-BA), with $m = 0, 1, 2, \ldots$. In fact, the only propagation direction we consider is x, along which on the average the magnetization is oriented ($\mathbf{k} \parallel \mathbf{M}$). At the Brillouin zone boundary, when $k = \frac{\pi}{d}$, modes m-BA and $(m+1)$-BA are out of phase of $\pi/2$, i.e., shifted of a quarter of their wavelength, and, hence, they experience differently the anisotropy field (e.g., 0-BA mode, i.e., the fundamental mode F, has nodes where the easy axis is at 0°, while 1-BA where it is at $\pm 45°$, see Fig. 4). This makes them no longer degenerate, and a frequency gap forms. As already remarked, the gap is forming only for $K_u \geq 0.4 \times 10^3\,\mathrm{J/m^3}$.

In our simulations, we found that the frequency gap increases with increasing K_u, and, after a first linear trend, tends to a saturation value of 0.9 GHz (Fig. 5). Being outside the purposes of the present investigation, we speculate that with an appropriate choice of materials, either the slope or the saturation values might be changed for specific purposes.

Finally, we underline an interesting effect: when the magnetic anisotropy becomes very large (e.g., $K_u \geq 2 \times 10^4\,\mathrm{J/m^3}$), the lowest frequency dispersion curve becomes progressively flatter,

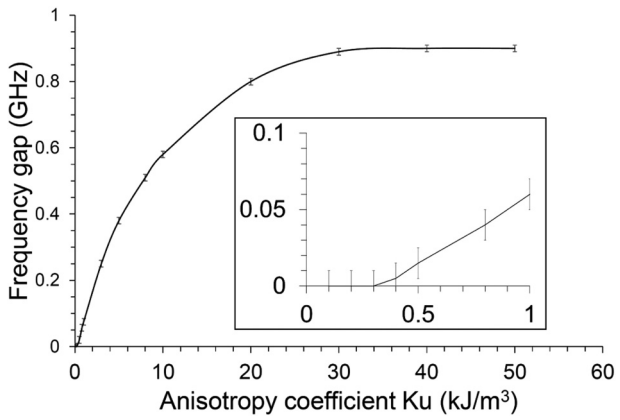

FIG. 5. Frequency gap resulting from the simulations as a function of the anisotropy coefficient K_u. A uniform error bar is shown, corresponding to 0.01 GHz (simulation resolution). The inset magnification shows how a gap is arising only beyond a threshold value ($K_u = 0.4 \times 10^3$ J/m^3).

while the higher dispersion curve maintains its parabolic shape. Hence, magnons belonging to the lower band become stationary (non-propagating resonances), while those belonging to the upper band are still propagating waves [Figs. 2(e) and 2(f)]. Once more this recalls analogies with electrons in semiconductors, which are bound and localized in the lower (valence) band and free and delocalized in the upper (conduction) band. The occurrence of either propagating or stationary modes in the same system at a tunable frequency gap is particularly interesting for signal filtering and manipulation.[61,62]

III. CONCLUSIONS

In conclusion, we devise a multiferroic magnonic crystal, which can be continuously (and reversibly) turned from a metal (zero gap, linear dispersion) to an insulator (significant gap, parabolic dispersion) for magnon propagation in real time with a single control parameter. The ultimate control parameter is the electric voltage applied to the FE overlayer. The FE domain distribution transfers vertically to the FM film through the inverse magnetoelastic effect, which we simulated through a magnetic anisotropy with an easy axis periodically varying in one direction, producing a sinusoidal distribution of the magnetization acting as a tunable magnonic crystal. The magnon gap width, group velocity, and effective mass can be effectively tuned by the (uniform) anisotropy coefficient in a wide range of values ($0-5 \times 10^4$ J/m^3). We extended the application of Dirac's magnon picture to a linear lattice in a continuous medium under the magnonic analog of metal (gapless) conditions ($0.04 < K_u < 0.4$ kJ/m^3), and we discussed how to control the hopping rate, which determines the magnon conductivity and is related to the strength of the overall interaction (exchange, dipolar, anisotropy). Under the magnon insulator conditions ($K_u \geq 0.4$ kJ/m^3), the emerging frequency gap was found to increase with increasing K_u, linearly at first, then gradually reaching saturation. Furthermore, we correlated the curvature of the parabolic dispersion branch to the magnon effective mass and found that the lower band tends to progressively reduce with increasing K_u up to become flat. In this way, films with sinusoidal magnetization at high K_u show the simultaneous presence of stationary and propagating magnons at a frequency distance close to 1 GHz: with this property, a suitable magnon can be excited to either carry or (dynamically) store information in the same physical magnonic device. Our results are particularly interesting for conceiving low-dissipation miniaturized devices involving ferromagnetic media and magnons as information carriers. Specifically, new magnonic devices based on voltage-controlled magnetic anisotropy and angular momentum transfer (magnons) would need no or extremely reduced electric currents and, hence, could be further miniaturized, at even large clock speeds, without the limitations due to Joule heating.

ACKNOWLEDGMENTS

P.M. and F.M. acknowledge support by the Department of Physics and Earth Sciences-University of Ferrara Grant Bando FIRD 2023, as well as the CINECA award under the ISCRA initiative, for the availability of high performance computing resources and support (Project SWIM-3D on Leonardo). A.R. and E.I. acknowledge support by the National Science Foundation (NSF) under Grant No. 2205796.

AUTHOR DECLARATIONS

Conflict of Interest

The authors have no conflicts to disclose.

Author Contributions

P. Micaletti: Writing – review & editing (equal). **A. Roxburgh:** Writing – review & editing (equal). **E. Iacocca:** Writing – review & editing (equal). **M. Marzolla:** Software (equal); Writing – review & editing (equal). **F. Montoncello:** Conceptualization (lead); Data curation (lead); Formal analysis (lead); Funding acquisition (lead); Investigation (lead); Methodology (lead); Software (equal); Supervision (lead); Writing – original draft (lead); Writing – review & editing (equal).

DATA AVAILABILITY

The data that support the findings of this study are available from the corresponding author upon reasonable request.

REFERENCES

[1]B. Rana and Y. Otani, "Towards magnonic devices based on voltage-controlled magnetic anisotropy," Commun. Phys. **2**(1), 90 (2019).
[2]L. Lannelongue, H.-E. G. Aronson, A. Bateman, E. Birney, T. Caplan, M. Juckes, J. McEntyre, A. D. Morris, G. Reilly, and M. Inouye, "Greener principles for environmentally sustainable computational science," Nat. Comput. Sci. **3**(6), 514–521 (2023).
[3]M. Mitchell Waldrop, "More than Moore," Nature **530**, 144–147 (2016).
[4]M. Mostovoy, "Multiferroics: Different routes to magnetoelectric coupling," npj Spintron. **2**(1), 18 (2024).

[5]A. B. Ustinov, A. V. Drozdovskii, A. A. Nikitin, A. A. Semenov, D. A. Bozhko, A. A. Serga, B. Hillebrands, E. Lähderanta, and B. A. Kalinikos, "Dynamic electromagnonic crystal based on artificial multiferroic heterostructure," Commun. Phys. **2**(1), 137 (2019).
[6]H. Qin, R. Dreyer, G. Woltersdorf, T. Taniyama, and S. van Dijken, "Electric-field control of propagating spin waves by ferroelectric domain-wall motion in a multiferroic heterostructure," Adv. Mater. **33**(27), 2100646 (2021).
[7]B. Van de Wiele, S. J. Hämäläinen, P. Baláž, F. Montoncello, and S. van Dijken, "Tunable short-wavelength spin wave excitation from pinned magnetic domain walls," Sci. Rep. **6**(1), 21330 (2016).
[8]M. E. Jamer, C. R. Rementer, A. Barra, A. J. Grutter, K. Fitzell, D. B. Gopman, J. A. Borchers, G. P. Carman, B. J. Kirby, and J. P. Chang, "Long-range electric field control of permalloy layers in strain-coupled composite multiferroics," Phys. Rev. Appl. **10**, 044045 (2018).
[9]T. H. E. Lahtinen, J. O. Tuomi, and S. van Dijken, "Pattern transfer and electric-field-induced magnetic domain formation in multiferroic heterostructures," Adv. Mater. **23**(28), 3187–3191 (2011).
[10]T. H. E. Lahtinen, K. J. A. Franke, and S. van Dijken, "Electric-field control of magnetic domain wall motion and local magnetization reversal," Sci. Rep. **2**(1), 258 (2012).
[11]S. J. Hämäläinen, M. Madami, H. Qin, G. Gubbiotti, and S. van Dijken, "Control of spin-wave transmission by a programmable domain wall," Nat. Commun. **9**, 4853 (2018).
[12]A. Barman, G. Gubbiotti, S. Ladak, A. O. Adeyeye, M. Krawczyk, J. Gräfe, C. Adelmann, S. Cotofana, A. Naeemi, V. I. Vasyuchka, B. Hillebrands, S. A. Nikitov, H. Y. D Grundler, A. V. Sadovnikov, A. A. Grachev, S. E. Sheshukova, J.-Y. Duquesne, M. Marangolo, G. Csaba, W. Porod, V. E. Demidov, S. Urazhdin, S. O. Demokritov, E. Albisetti, D. Petti, R. Bertacco, H. Schultheiss, V. V. Kruglyak, V. D. Poimanov, S. Sahoo, J. Sinha, H. Yang, M. Münzenberg, T. Moriyama, S. Mizukami, P. Landeros, R. A. Gallardo, G. Carlotti, J.-V. Kim, R. L. Stamps, R. E. Camley, B. Rana, Y. Otani, W. Y. T Yu, G. E. W Bauer, C. Back, G. S. Uhrig, O. V. Dobrovolskiy, B. Budinska, H. Qin, S. van Dijken, A. V. Chumak, A. Khitun, D. E. Nikonov, I. A. Young, B. W. Zingsem, and M. Winklhofer, "The 2021 magnonics roadmap," J. Phys.: Condens. Matter **33**(41), 413001 (2021).
[13]T. Dion, K. D. Stenning, A. Vanstone, H. H. Holder, R. Sultana, G. Alatteili, V. Martinez, M. T. Kaffash, T. Kimura, R. F. Oulton, W. R. Branford, H. Kurebayashi, E. Iacocca, M. B. Jungfleisch, and J. C. Gartside, "Ultrastrong magnon-magnon coupling and chiral spin-texture control in a dipolar 3D multilayered artificial spin-vortex ice," Nat. Commun. **15**(1), 4077 (2024).
[14]R. Negrello, F. Montoncello, M. T. Kaffash, M. B. Jungfleisch, and G. Gubbiotti, "Dynamic coupling and spin-wave dispersions in a magnetic hybrid system made of an artificial spin-ice structure and an extended NiFe underlayer," APL Mater. **10**, 091115 (2022).
[15]F. Montoncello, M. T. Kaffash, H. Carfagno, M. F. Doty, G. Gubbiotti, and M. B. Jungfleisch, "A Brillouin light scattering study of the spin-wave magnetic field dependence in a magnetic hybrid system made of an artificial spin-ice structure and a film underlayer," J. Appl. Phys. **133**, 083901 (2023).
[16]X. R. Wang, X. Gong, and K. Y. Jing, "Supermirrors and spin wave amplifications," Appl. Phys. Lett. **124**(8), 082403 (2024).
[17]L. C. Parsons, "Influence of spin wave attenuation on a ferromagnetic nanowire-based magnonic Bragg mirror," J. Magn. Magn. Mater. **426**, 794–799 (2017).
[18]R. Huber, T. Schwarze, and D. Grundler, "Nanostripe of subwavelength width as a switchable semitransparent mirror for spin waves in a magnonic crystal," Phys. Rev. B **88**, 100405 (2013).
[19]J. D. Joannopoulos, S. G. Johnson, J. N. Winn, and R. D. Meade, *Photonic Crystals: Molding the Flow of Light*, 2nd ed. (Princeton University Press, 2008).
[20]P. Bhattacharjee and S. Barman, "Control of band gap of spin waves in width-modulated nanostrip using voltage-controlled magnetic anisotropy: Spin wave filter," in *2023 Second International Conference on Electrical, Electronics, Information and Communication Technologies (ICEEICT)* (IEEE, 2023), pp. 1–4.
[21]P. Frey, A. A. Nikitin, D. A. Bozhko, S. A. Bunyaev, G. N. Kakazei, A. B. Ustinov, B. A. Kalinikos, F. Ciubotaru, A. V. Chumak, Q. Wang, V. S. Tiberkevich, B. Hillebrands, and A. A. Serga, "Reflection-less width-modulated magnonic crystal," Commun. Phys. **3**(1), 17 (2020).
[22]Q. Wang, A. V. Chumak, L. Jin, H. Zhang, B. Hillebrands, and Z. Zhong, "Voltage-controlled nanoscale reconfigurable magnonic crystal," Phys. Rev. B **95**, 134433 (2017).
[23]C.-G. Duan, J. P. Velev, R. F. Sabirianov, Z. Zhu, J. Chu, S. S. Jaswal, and E. Y. Tsymbal, "Surface magnetoelectric effect in ferromagnetic metal films," Phys. Rev. Lett. **101**, 137201 (2008).
[24]M. Staruch, D. B. Gopman, Y. L. Iunin, R. D. Shull, S. F. Cheng, K. Bussmann, and P. Finkel, "Reversible strain control of magnetic anisotropy in magnetoelectric heterostructures at room temperature," Sci. Rep. **6**(1), 37429 (2016).
[25]M. Balinskiy, A. C. Chavez, A. Barra, H. Chiang, G. P. Carman, and A. Khitun, "Magnetoelectric spin wave modulator based on synthetic multiferroic structure," Sci. Rep. **8**(1), 10867 (2018).
[26]S. Mamica, X. Zhou, A. Adeyeye, M. Krawczyk, and G. Gubbiotti, "Spin-wave dynamics in artificial anti-spin-ice systems: Experimental and theoretical investigations," Phys. Rev. B **98**, 054405 (2018).
[27]E. Iacocca, S. Gliga, R. L. Stamps, and O. Heinonen, "Reconfigurable wave band structure of an artificial square ice," Phys. Rev. B **93**, 134420 (2016).
[28]S. S. Pershoguba, S. Banerjee, J. C. Lashley, J. Park, H. Ågren, G. Aeppli, and A. V. Balatsky, "Dirac magnons in honeycomb ferromagnets," Phys. Rev. X **8**, 011010 (2018).
[29]A. V. Chumak, A. A. Serga, and B. Hillebrands, "Magnonic crystals for data processing," J. Phys. D: Appl. Phys. **50**(24), 244001 (2017).
[30]A. K. Dhiman, N. Leśniewski, R. Gieniusz, J. Kisielewski, P. Mazalski, Z. Kurant, M. Matczak, F. Stobiecki, M. Krawczyk, A. Lynnyk, A. Maziewski, and P. Gruszecki, "Reconfigurable magnonic crystals: Spin wave propagation in Pt/Co multilayer in saturated and stripe domain phase," APL Mater. **12**(11), 111106 (2024).
[31]F. Ma, Y. Zhou, H. B. Braun, and W. S. Lew, "Skyrmion-based dynamic magnonic crystal," Nano Lett. **15**(6), 4029–4036 (2015).
[32]P. Micaletti, A. Roxburgh, E. Iacocca, M. Marzolla, and F. Montoncello, "A sinusoidal magnetization distribution as an original way to generate a versatile magnonic crystal for magnon propagation," J. Magn. Magn. Mater. **622**, 172959 (2025).
[33]A. V. Chumak, T. Neumann, A. A. Serga, B. Hillebrands, and M. P. Kostylev, "A current-controlled, dynamic magnonic crystal," J. Phys. D: Appl. Phys. **42**(20), 205005 (2009).
[34]M. Vogel, A. V. Chumak, E. H. Waller, T. Langner, V. I. Vasyuchka, B. Hillebrands, and G. von Freymann, "Optically reconfigurable magnetic materials," Nat. Phys. **11**, 487–491 (2015).
[35]R. G. Kryshtal and A. V. Medved, "Surface acoustic wave in yttrium iron garnet as tunable magnonic crystals for sensors and signal processing applications," Appl. Phys. Lett. **100**(19), 192410 (2012).
[36]R. G. Kryshtal and A. V. Medved, "Surface acoustic waves in dynamic magnonic crystals for microwave signals processing," Ultrasonics **94**, 60–64 (2019).
[37]I. A. Ustinova, A. A. Nikitin, and A. B. Ustinov, "Dynamic magnonic crystal based on a layered ferrite–ferroelectric structure," Tech. Phys. **61**(3), 473–476 (2016).
[38]A. A. Nikitin, N. Kuznetsov, S. van Dijken, and E. Lähderanta, "Dynamic electromagnonic crystals based on ferrite-ferroelectric thin film multilayers," Phys. Rev. B **109**, 024440 (2024).
[39]A. A. Nikitin, A. E. Komlev, A. A. Nikitin, A. B. Ustinov, and E. Lähderanta, "Dynamic magnonic crystals based on vanadium dioxide gratings," Phys. Rev. Appl. **20**, 044026 (2023).
[40]V. E. Demidov, B. A. Kalinikos, and P. Edenhofer, "Dipole-exchange theory of hybrid electromagnetic-spin waves in layered film structures," J. Appl. Phys. **91**(12), 10007–10016 (2002).
[41]A. A. Nikitin, A. B. Ustinov, V. V. Vitko, A. A. Semenov, P. Y. Belyavskiy, I. G. Mironenko, A. A. Stashkevich, B. A. Kalinikos, and E. Lähderanta, "Dispersion characteristics of spin-electromagnetic waves in planar multiferroic structures," J. Appl. Phys. **118**(18), 183901 (2015).

[42]A. Vansteenkiste, J. Leliaert, M. Dvornik, M. Helsen, F. Garcia-Sanchez, and B. Van Waeyenberge, "The design and verification of MuMax3," AIP Adv. **4**(10), 107133 (2014).
[43]R. O. Serha, A. A. Voronov, D. Schmoll, R. Verba, K. O. Levchenko, S. Koraltan, K. Davídková, B. Budinská, Q. Wang, O. V. Dobrovolskiy, M. Urbánek, M. Lindner, T. Reimann, C. Dubs, C. Gonzalez-Ballestero, C. Abert, D. Suess, D. A. Bozhko, S. Knauer, and A. V. Chumak, "Magnetic anisotropy and GGG substrate stray field in YiG films down to millikelvin temperatures," npj Spintron. **2**(1), 29 (2024).
[44]D. Lebeugle, A. Mougin, M. Viret, D. Colson, and L. Ranno, "Electric field switching of the magnetic anisotropy of a ferromagnetic layer exchange coupled to the multiferroic compound $BiFeO_3$," Phys. Rev. Lett. **103**, 257601 (2009).
[45]The z-component is usually relevant in the experiments, either ferromagnetic resonance or Brillouin light scattering.
[46]C. Kittel and P. McEuen, *Introduction to Solid State Physics* (John Wiley & Sons, 2015).
[47]F. Montoncello and G. Gubbiotti, "Controlling the three dimensional propagation of spin waves in continuous ferromagnetic films with an increasing out of plane undulation," Sci. Rep. **11**, 21344 (2021).
[48]B. A. Kalinikos and A. N. Slavin, "Theory of dipole-exchange spin wave spectrum for ferromagnetic films with mixed exchange boundary conditions," J. Phys. C: Solid State Phys. **19**(35), 7013 (1986).
[49]R. W. Damon and J. R. Eshbach, "Magnetostatic modes of a ferromagnet slab, J. Phys. Chem. Solids **19**(3), 308–320 (1961).
[50]G. Gubbiotti, L. L. Xiong, F. Montoncello, L. Giovannini, and A. O. Adeyeye, "Spin wave dispersion and intensity correlation in width-modulated nanowire arrays: A Brillouin light scattering study," J. Appl. Phys. **124**, 083903 (2018).
[51]K. J. A. Franke, B. Van de Wiele, Y. Shirahata, S. J. Hämäläinen, T. Taniyama, and S. van Dijken, "Reversible electric-field-driven magnetic domain-wall motion," Phys. Rev. X **5**, 011010 (2015).
[52]Z. Zhou, B. M. Howe, M. Liu, T. Nan, X. Chen, K. Mahalingam, N. X. Sun, and G. J. Brown, "Interfacial charge-mediated non-volatile magnetoelectric coupling in $Co_{0.3}Fe_{0.7}/Ba_{0.6}Sr_{0.4}TiO_3/Nb:SrTiO_3$ multiferroic heterostructures," Sci. Rep. **5**(1), 7740 (2015).
[53]S. Homkar, D. Preziosi, X. Devaux, C. Bouillet, J. Nordlander, M. Trassin, F. Roulland, C. Lefèvre, G. Versini, S. Barre, C. Leuvrey, M. Lenertz, M. Fiebig, G. Pourroy, and N. Viart, "Ultrathin regime growth of atomically flat multiferroic gallium ferrite films with perpendicular magnetic anisotropy," Phys. Rev. Mater. **3**, 124416 (2019).
[54]T. H. E. Lahtinen, Y. Shirahata, L. Yao, K. J. A. Franke, G. Venkataiah, T. Taniyama, and S. van Dijken, "Alternating domains with uniaxial and biaxial magnetic anisotropy in epitaxial Fe films on $BaTiO_3$," Appl. Phys. Lett. **101**(26), 262405 (2012).
[55]M. Tinkham, *Group Theory and Quantum Mechanics* (Dover Publications, 2003).
[56]V. Ariel and A. Natan, "Electron effective mass in graphene," in *2013 International Conference on Electromagnetics in Advanced Applications (ICEAA)* (IEEE, 2013), pp. 696–698.
[57]J. Fransson, A. M. Black-Schaffer, and A. V. Balatsky, "Magnon Dirac materials," Phys. Rev. B **94**, 075401 (2016).
[58]L. Giovannini, "Dirac magnons in honeycomb nanostructures," Phys. Rev. B **107**, 104418 (2023).
[59]G. Venkat, D. Kumar, M. Franchin, O. Dmytriiev, M. Mruczkiewicz, H. Fangohr, A. Barman, M. Krawczyk, and A. Prabhakar, "Proposal for a standard micromagnetic problem: Spin wave dispersion in a magnonic waveguide," IEEE Trans. Magn. **49**, 524 (2013).
[60]M. El-Batanouny, *Advanced Quantum Condensed Matter Physics: One-Body, Many-Body, and Topological Perspectives* (Cambridge University Press, 2020).
[61]A. Frotanpour, J. Woods, B. Farmer, A. P. Kaphle, L. E. De Long, L. Giovannini, and F. Montoncello, "Magnetization dynamics of a Fibonacci-distorted Kagome artificial spin ice," Phys. Rev. B **102**, 224435 (2020).
[62]A. Mahmoud, F. Ciubotaru, F. Vanderveken, A. V. Chumak, S. Hamdioui, C. Adelmann, and S. Cotofana, "Introduction to spin wave computing," J. Appl. Phys. **128**, 161101 (2020).